Large spin accumulation signals in ultrafast magneto-optical experiments.

Alberto Anadón,[1,2,*] Harjinder Singh,[1,†] Eva Díaz,[1] Yann Le-Guen,[1] Julius Hohlfeld,[1] Richard B. Wilson,[3] Gregory Malinowski,[1] Michel Hehn,[1] and Jon Gorchon[1,‡]

[1] *Université de Lorraine, CNRS, IJL, Nancy, F-54000, France*
[2] *Instituto de Nanociencia y Materiales de Aragón (INMA), CSIC-Universidad de Zaragoza, Zaragoza 50009, Spain*
[3] *Department of Mechanical Engineering and Materials Science and Engineering Program, University of California, Riverside, CA, USA*

(Dated: October 23, 2025)

Magneto-optical techniques have become essential tools in spintronics, enabling the investigation of spin dynamics in the ultrafast regime. A key challenge in this field has been to accurately isolate the contributions to magneto-optical signals of spin transport phenomena from the local magnetization dynamics. The contribution of transported and accumulated spins was long believed to be orders of magnitude smaller than that of the magnetization and thus previous approaches to disentangle these signals have relied on specific experimental designs, usually including thick metal layers. Here, we present experimental evidence demonstrating that the magneto-optical signal from ultrafast spin accumulations can, under certain conditions, be comparable to or even exceed that of the magnetic layer in a standard ultrafast demagnetization experiment. Our findings provide a new framework for accessing and isolating these spin accumulations, allowing for time and depth dependent probing of transported spin and/or orbital angular momentum.

INTRODUCTION

Historically, magneto-optical probes have played a vital role in unveiling and exploring various spintronic phenomena [1–7]. Furthermore, in combination with femtosecond laser sources, magneto-optics offers a direct window into ultrafast spin dynamics [8–10]. Typical experiments consist of a first intense femtosecond-wide laser pulse which excites (i.e. pumps) a magnetic system, and a second lower-fluence one which probes the changes in the magnetic system via the magneto-optical Kerr effect (MOKE). During excitation electrons absorb the optical energy, which then gets redistributed locally among other electrons, phonons and spins, and non-locally as it is transported into neighboring layers. This redistribution of energy also results in a redistribution of angular momentum, and may result in the generation of ultrafast spin currents. In fact, such spin currents are nowadays paramount for the understanding of all-optical magnetization switching [9, 11] and broadband spintronic THz emitters [12].

While advances on alternate probes such as THz emission [13, 14], ultrafast X-ray based methods [15, 16], or time-resolved photoemission [17] have undoubtedly confirmed the loss of magnetization and presence of THz spin currents, MOKE remains the most widely used method to characterize ultrafast magnetization dynamics. However, the role of Kerr rotation θ_k and ellipticity ϵ_k and its connection with the magnetic properties of thin films in the ultrafast regime is still somewhat controversial. In 2000, Koopmans et al. found a significant difference between θ_k and ϵ_k in the first picoseconds after the excitation of a Ni thin film grown on a Cu(111) substrate [18], ascribing the differences to non-magnetic optical contributions. In contrast, Guidoni et al. soon after showed that in a $CoPt_3$ film grown on sapphire the θ_k and ϵ_k had the same time evolution [19]. Many more works tried to test the validity of MOKE at the time, both experimentally and

theoretically, with no clear consensus [20–24]. Noting the use of conductive Cu substrates [18] vs sapphire [19], some works have since argued that the observed differences are likely related to spin transport and have attempted to probe and model the depth profile of the magnetization by carefully comparing θ_k and ϵ_k signals [25, 26]. Other works have attempted to probe directly the resulting spin accumulation directly via linear and non-linear MOKE on thick and opaque non-magnetic layers [27–32]. By using such thick layers, the authors could avoid the probe from reaching the magnetic layer. Notably, Hofherr et al.[33] attempted to disentangle the spin accumulation and demagnetization MOKE signals in a Ni/Au bilayer by shining the probe directly on the ferromagnetic layer. This was achieved by cleverly mixing the θ_k and ϵ_k with a quarter wave-plate and suppressing the MOKE contribution from the Ni layer. Unfortunately, likely due to the limited signal-to-noise ratio, this experiment has not been reproduced yet. In fact, to this day, spin accumulation signals have never been considered as an important contribution to MOKE in usual TR-MOKE experiments.

Here we demonstrate that, under certain common conditions, spin accumulation signals can be as large or even larger than the magneto-optical signals attributed to the magnetic layer, leading to possibly confusing interpretations. By studying a series of wedged magnetic/non-magnetic bilayer systems we are able to directly probe the pure demagnetization, spin accumulation or a mixed signal, and deconvolute each contribution. We also show that differences between MOKE rotation and ellipticity may arise from the magneto-optical signal due to spin accumulation. In the case of Cu, we show that ellipticity is a much better probe of the demagnetization dynamics in the ferromagnet, whereas the rotation signal contains an important sensitivity to spin accumulation. Importantly, we demonstrate that the spin accumulation signal can also be sizable in experiments with low repetition rate amplified systems, opening the door for spin accumulation detection with most pulsed laser systems and up to extreme fluences. Strikingly, we are able to generate and measure spin accumulations up to half a mrad, on the order of full magneto-optical signals of common ferromagnets, despite the low spin-orbit coupling in Cu. All our measurements are reasonably well fitted by an ultrafast spin-diffusion model, which includes magneto-optical sensitivities based on a transmission matrix model. Our results open the door to new ways to detect spin (or orbital) angular momentum in common systems and should improve the interpretation of MOKE signals.

METHODS

Sample growth. Samples were prepared using magnetron sputtering in an Ar atmosphere of 4x10^{-3} mbar and with a base pressure less then 2x10^{-8} mbar. In this study double sided polished sapphire substrates were used for depositing the thin films. The primary FM stack used in this study is Ta(3)Cu(5)[Ni(0.7)/Co(0.2)]$_4$ and referred to as Co/Ni. The values inside parentheses are thicknesses in nm. Three different wedge samples were fabricated with the magnetic stack of Co/Ni: Co/Ni/Cu(t)/Al(3) by varying the Cu thickness within the following ranges: 10 to 30 nm (wedge-1), 20 to 60 nm (wedge-2), and 50 to 150 nm (wedge-3). All the samples have perpendicular magnetic anisotropy (PMA). To protect the topmost Cu layer from the oxidation the samples have thin protective layer of Al that passivates in contact with the air. (See supplementary for more details about wedge samples. See also references [30, 35–43] therein). Moreover, besides Co/Ni, we deposited other magnetic stack: Ta(3)/Pt(10)/[Co(0,82)/Pt(1)]$_2$/Co(0,82) referred to as Co/Pt.

To study the effect of the capping layer on spin accumulation, we deposited samples both with and without an Al capping layer: Co/P-

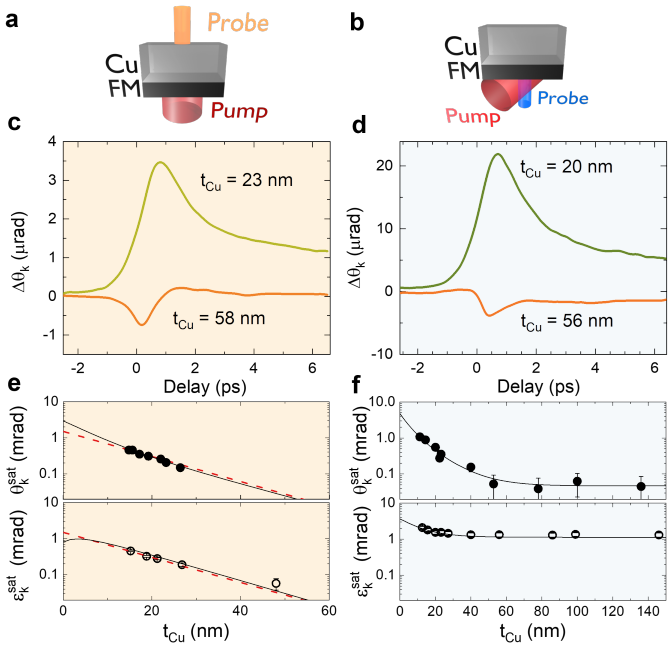

FIG. 1. **Experimental configuration, as well as time-resolved and static magneto-optical Kerr responses in the CoNi/Cu structures. a,b** shows Schematic for the two different experimental configurations where the pump is always incident on the FM-side (through the sapphire substrate), whereas the probe is incident either on the **a** Cu-side or **b** the FM-side. Time-resolved magneto-optical measurements with the pump beam always directed towards the FM side and the probe beam is directed to the Cu **c** and CoNi **d** sides for two different Cu thickness. We see that the peak in both cases changes sign and shows at a lower delay time for the thicker Cu. **e** and **f** panels show the rotation and ellipticity at saturation (no incident pump) from the Cu side **e** and the FM side **f** as a function of the Cu thickness. The dashed red lines in **e** are an exponential decay fit to the data, while the continuous black likes are a fits using a transmission-matrix-method simulation[34]. If error bars are not indicated in the graphs, they are within the point.

t/Cu(100)/Al(2.5) and Co/Pt/Cu(100) respectively. Additionally, a wedge sample using Co/Ni as FM: Co/Ni/Cu(100)/Al(t) by varying Al thickness ranges from 2 to 30 nm was also fabricated.

In addition to this, we have also studied spin accumulation in materials other than Cu. For this we have deposited samples with Co/Pt as FM but Al as NM with the following stack: Co/Pt/Al(80) and Co/Pt/Al(80)/Au(5), Co/Pt/Cu(100)/Pt(5), Co/Pt/Cu(100)/Ta(5).

Experimental setups. Two different Ti:sapphire femtosecond lasers were used.

The main laser system is a Chameleon Vision-S® (from Coherent®) oscillator with a repetition rate of 80 MHz, a 785 nm center wavelength and a 12 nm bandwidth. We separate pump and probe beams by using very sharp edge-filters (Semrock® SP01-785RU and LP02-785RE) which split the spectrum and avoid possible interference effects between pump and probe. The pump pulse-duration after spectrum filtering was measured at around 100 fs whereas the probe is at around 600 fs. The

pump has a gaussian profile with a full width half maximum of around 50±2 μm. When the pump is incident at 45°(Cu-side experiments), the full-width half maximum is estimated at 50 μm. The probe is focused through a long-working distance objective resulting in a size of around 5μm. We used for all experiments a pump power of 180mW, resulting in an incident fluence of around 0.1 mJ/cm^2. We used a quarter-wave plate to change the probe sensitivity from rotation to ellipticity (see Suppl. Mat.[34] S5-6). For determining the saturation rotation and ellipticities, we use a chopper to modulate the probe (for lock-in detection), block the pump and perform hysteresis cycles. The values θ_k^{sat} and ϵ_k^{sat} correspond to the half difference between traces obtained for positive and negative saturation fields. For pump probe experiments we modulate the pump at 1.1 MHz with an electro-optic modulator. Reported $\Delta\theta_k$ and $\Delta\epsilon_k$ correspond to the half difference for measurements with opposite saturated states. For more details on the signal analysis (see Suppl. Mat.[34] Sec 5-6).

The second setup, used for data shown in Fig.5, is a Legend® regenerative amplified laser (from Coherent®) with a repetition rate of 5 KHz and pulse width of 25 fs. The pump and probe wavelengths are centered at 800 nm and 400 nm respectively, by using a BBO crystal to double the probe. The full beam width at $1/e^2$ of the pump is 243±9 μm whereas for the probe it is around 50μm. The pump is incident at normal incidence, whereas the probe is incident at a few degrees away from normal incidence.

Magnetic field during experiments. In all experiments, an out of plane magnetic field is applied only to saturate the ferromagnetic layer and is turned off during the measurement. In Suppl. Mat. S9) we show possible artifacts in some configurations due to presence of the magnetic field during scans. The strength of the applied field is larger than the coercive field of the magnetic layer. Presented experimental data always corresponds to the half difference between traces obtained for positive and negative saturation fields. In a few instances, at very high powers (inset of Fig.5b), the field is maintained constant during experiments to reset the magnetization between pulses.

Zero time delay accuracy. We note that the zero delay between Cu-side and FM-side experiments is different due to the differences in the optical paths used, and has been arbitrarily defined. For FM-side experiments, the sample position does not affect the zero delay, as both pump and probe travel in the same direction and will experience the same shift in delay. However, in back-front type experiments, for the Cu-side experiments, any shift in sample position affects the arrival time of both the pump and probe beams in an opposite way. Therefore a shift of Δx in sample position, will result in a shift in $2\Delta x/c$ in zero delay, c being the speed of light. On the one hand, on the 80 MHz setup, benefiting from the shallow depth-of-field of the objective, the accuracy on the sample position is around 5 μm, resulting in an uncertainty of around 30 fs. On the other hand, with the 5 kHz setup, we estimate the positional uncertainty to be around 200 μm, resulting in large shifts reaching the picosecond . For this reason, temporal shifts should not be compared on Fig.5 when the sample is changed.

RESULTS

Setup and samples: We fabricated three wedged samples of sapphire//Ta(3)/Cu(5)/[Ni(0.7)/Co(0.2)]$_4$Cu(t_{Cu})/Al(3), where the thickness appears in parenthesis, expressed in nanometers. The Cu layer of the three samples has a variable thickness t_{Cu} ranging from 10 to 30 nm, 20 to 60 nm and 50 to 150 nm, for the three samples (see End Matter). All Co/Ni multilayers have a perpendicular magnetic anisotropy. The top Al layer should be naturally passivated and was added to protect the Cu from oxidation. For simplicity, from here on, we will refer to the ferromagnetic Ta/Cu/[Co/Ni] section of the

stack as the *FM-side*, and to the top Cu/Al stack as the *Cu-side*. Most experiments were carried out with an 80 MHz Ti-Sa laser system which provides pulses of a few nanojoules, at a 785 nm wavelength, with a time resolution of around 0.6 ps (see End Matter). Alternatively, a 5 KHz 25 femtosecond amplified Ti-Sa system was also used, where the probe wavelength was halved to 400 nm (see End Matter).

Dynamic magneto-optics: We first performed pump-probe time-resolved magneto-optical Kerr effect (TR-MOKE) experiments with the 80 MHz laser system. Experiments were performed by exciting (i.e. pumping) the FM side through the transparent substrate, and probing on both the sides of the sample at normal incidence, in polar MOKE configuration, as depicted in Figs.**1a-b**. For easy identification of the experiment configuration, when probing the Cu side we identify the graphs by an orange background shade, whereas when probing through the FM side the shade is blue. In Figs.**1c** and **d**, we plot the change in Kerr rotation induced by the pump beam $\Delta\theta_k$ as a function of pump-probe delay.

As shown in Figs.**1c**, t_{Cu}=23 nm is thin enough that the probe can still see the magnetic layer through the Cu layer, and we observe a typical demagnetization trace[8], showing a first rapid drop in magnetization and a subsequent slower recovery as the magnetic system cools down. We remind the reader here that the plotted sign of the magneto-optical change is not absolute, as it depends on the optical detection path configuration, magnetization direction with respect to the light's **k** vector, optical constants and arbitrary conventions (such as the choice of the sign of a clock-wise rotation). However, for a given setup configuration, signs of different datasets can be compared. When the thickness is increased to t_{Cu}=58 nm, light reaching the magnetic layer is drastically reduced and therefore, as previously shown[44], the magneto-optical signal can safely be attributed to the spin accumulation resulting from the ultrafast spin currents generated during demagnetization (see [34] for measurements up to 200 nm in Cu thickness).

To probe through the FM-side, the sample is flipped and the pump is changed to keep exciting the FM-side, but the electromagnet and probe path are not modified. As seen in Fig. **1d** for t_{Cu}=20 nm, we also observe a typical demagnetization trace. However, for t_{Cu}=56 nm, we can see that the trace changes significantly, showing a peak with different timing, opposite polarity and lower amplitude. In this configuration, the Cu layer does not prevent the probe from reaching the magnetic layer, making these changes unexpected.

Static magneto-optics: We therefore investigated the static magneto-optical signals of the multilayer by probing the saturation Kerr rotation θ_k^{sat} and ellipticity ε_k^{sat} (i.e. the half-amplitude of the hysteresis cycle) as a function of t_{Cu}, from both the Cu and FM sides. As shown in Fig.**1e**, when probing the Cu-side, both θ_k^{sat} and ε_k^{sat} follow the expected Beer-Lambert-like exponential decay (red dashed line) given by $e^{-2\pi\lambda^{-1}\mathrm{k_{Cu}}2t_{Cu}}$, where $\mathrm{k_{Cu}}$ is the imaginary part of the optical index of Cu, λ is the optical wavelength in vacuum, and $2t_{Cu}$ includes both the forward and reflected backward propagation of the electric field through the Cu layer[45]. Since θ_k^{sat} is divided by 10 when t_{Cu} is changed from 23 nm to 58 nm, the orange curve in Fig.**1c** stills contains a very small contribution of the ferromagnet's magneto-optical signal. When probing from the FM-side, we observe that θ_k^{sat} is reduced by more than an order of magnitude as t_{Cu} increases past 50 nm. This is not the case for ε_k^{sat}, where a smaller decay is observed, but the value remains at around 1 mrad.

Magneto-optical model: To model the magneto-optical signals we used a generalized transmission-matrix-model with non-diagonal susceptibility terms [34, 46, 47] determined by the complex magneto-optical Voigt constants **Q**. All diagonal (non-magnetic) susceptibility terms where fixed from literature values, and the magnetic layer's $\mathbf{Q}_{Co/Ni}$ was fitted result-

ing in the solid lines shown in panels Figs.**1e,f**. We obtained a value of $\mathbf{Q}_{Co/Ni}$=0.012-0.016i (±5%), in good agreement with values from Ref.[48]. The extremely good fit allows us to predict the evolution of the magneto-optical signal as a function of thickness with high accuracy. We attribute most of θ_k^{sat} at low t_{Cu} to the wave that propagates and gains Faraday rotation through the ferromagnetic layer which is back-reflected on the Cu/Al_2O_3 interface. As this interface is moved away by increasing t_{Cu}, its contribution is reduced. All other multi-reflections within the structure remain equal, which means that to cancel the total rotation, the transverse reflected fields must destructively interfere.

Full thickness dependence: The full t_{Cu} dependence of $\Delta\theta_k$ for both Cu-side and FM-side configurations is depicted in Figs. **2a-d**. In Fig.**2a** we show that as t_{Cu} increases from 11 to 27 nm, the peak $\Delta\theta_k$ is reduced due to the reduction in magneto-optical sensitivity of the FM (see Fig.**1e**). At t_{Cu} = 40 nm, the trace becomes bipolar due to the emergence of a new earlier negative peak, which we associate with spin accumulation. Fig.**2b** shows a closeup of the 40 nm trace, and its evolution as t_{Cu} increases up to 139 nm. For higher t_{Cu}, the magneto-optical signal from the FM is drastically reduced, and only a pure spin accumulation signal remains, in agreement with previous works [27–29, 32, 44]. The decreasing amplitude and increasing delay time of the negative peak is related to the diffusive transport of the angular momentum in the Cu film, from which an average velocity of 0.17 nm/fs can be extracted[34] (a fraction of the usual 1 nm/fs Fermi velocity).

Fig.**2c** shows the $\Delta\theta_k$ from 11 to 40 nm when probing the FM-side. Similarly, we see a reduction of the peak $\Delta\theta_k$ as the magneto-optical sensibility to the FM is reduced with the increase of t_{Cu} (see Fig.**1f**). Around t_{Cu} = 27 nm we start to see a change in the shape of the trace, with a negative peak forming, which we *also* attribute to spin accumulation. At thicker t_{Cu} (Fig.**2d**) this negative signal increases, reaching a maximum at $t_{Cu} \approx 60$ nm. Despite the probe impinging the FM-side, the increase in t_{Cu} and reduction in θ_k^{sat} results in a larger sensitivity to the spin accumulation *behind* the FM, rather than to the magnetization of the FM itself. Potentially, spin accumulation within the ferromagnet could also contribute to this magneto-optical signal. Interestingly, we believe the long-lived tail in Fig.**2d** is likely linked to the spin-dependent Seebeck effect as previously suggested[29]. We observed similar but smaller amplitude long-lived signal when probing through the Cu-side as studied in Ref.[29]. Importantly, most literature works assume that many ps after optical excitation, artifacts in θ_k signals can be safely excluded. Our data clearly shows this is not always true, and therefore care should be taken when, for example, using a magnet as a transducer for temperature estimations in metals[29, 49–51]. If the normalized dynamics $\Delta\theta_k/\theta_k^{sat}$ and $\Delta\epsilon_k/\epsilon_k^{sat}$ do not match[18], the differences might be due to spin accumulation in the neighboring metal and should not be attributed to magnetization. This possible mismatch depends strongly on the specific combination of materials and probe conditions, and remains to be further explored.

Finally, in the lower panels **e** and **f** of Fig.2, we show the derivative with respect to the delay time for the curve with t_{Cu} = 11 nm (dM/dt) shown in panels **a** and **b**, respectively, which follow the demagnetization. Based on prevailing theories for spin-current generation by ultrafast demagnetization, the peak of the dM/dt should correspond with the maximum of the spin current generation[29], which we identify by a gray shaded area. As can be seen, for a Cu-side probe (Fig.2.b), the spin accumulation peak for the thinnest layers coincides with the dM/dt peak, and is delayed as the Cu layer is made thicker [52]. However, for the FM-side probe, we observe a small constant delay. This delay is constant because, due the limited penetration depth in Cu, we are measuring the interface in contact with the FM, which does not change with t_{Cu}, but the origin of the delay is

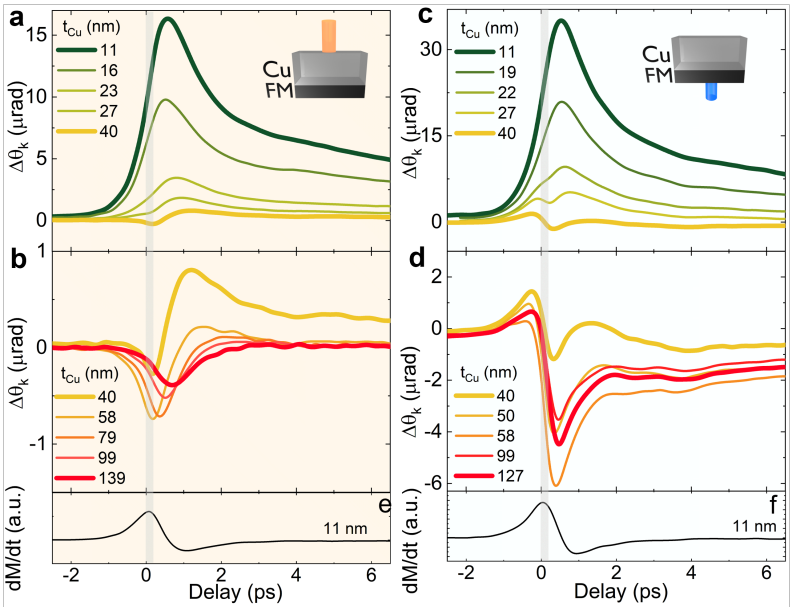

FIG. 2. **Mixed demagnetization and spin accumulation signals in CoNi/Cu(t).** TR-MOKE signal for varying Cu thickness with the probe beam incident on the **a,c** CoNi layer side and the **b,d** Cu layer side. At lower t_{Cu}, the curves for both configurations resemble a classical demagnetization curve. At medium thickness, an additional peak appears, pointing downward in both cases. At higher t_{Cu}, this peak clearly dominates over the demagnetization peak. At high Cu thickness, when the probe hits the Cu side, a mostly symmetric peak is observed, and $\Delta\theta_k$ returns to zero after a few picoseconds. In the configuration where the probe hits the CoNi layer, the peak is clearly asymmetric and a flat background is observed after the peak. Panels **e** and **f** show the derivative with respect to the delay time of the curve with $t_{Cu} = 11$ nm for both probe configurations. The grey shaded areas represent the peaks of the curves in panels **e** and **f**.

not yet clear.

Rotation vs ellipticity: In Fig.**3** we show the comparison between $\Delta\theta_k$ and $\Delta\epsilon_k$ signals for a few selected thicknesses. On the one hand, $\Delta\theta_k$ follows the previously described trends, probing either the magnetization (Figs.**3a,d**), the spin accumulation (Figs.**3c,f**) or a mixture of both (Figs.**3b,e**). $\Delta\epsilon_k$ on the other hand, generally shows a demagnetization like trace (Figs.**3a,b,d,e,f**) with a decaying amplitude as t_{Cu} is increased[54]. At t_{Cu}= 140 nm (Figs.**3c**) the sensitivity to the magnetic layer is orders of magnitude lower, so that we could attribute any sizeable signal to the spin accumulation in the Cu layer. From it, we can determine the sensitivity of ϵ_k to spin accumulation in the Cu, which is drastically lower than that of θ_k (in agreement with Ref.[32, 55]). Therefore, in order to measure the actual magnetization dynamics one has to be careful with the sensitivities to spin accumulation, and in the case of Cu, a measurement of ϵ_k should give the best results when using a wavelength of around 800 nm. While the magneto-optical signal that we find in Cu is surprisingly large for a material with low spin-orbit coupling, it is compatible with values obtained in previous studies[32]. As reference, we note that the atomic spin-orbit splitting in Co and Ni ferromagnets is close to 0.1 eV[56] and results in important magneto-optical signals, while in Cu it is 0.25eV for Cu3d and 0.03eV for Cu4p[28, 57] , which is not dras-

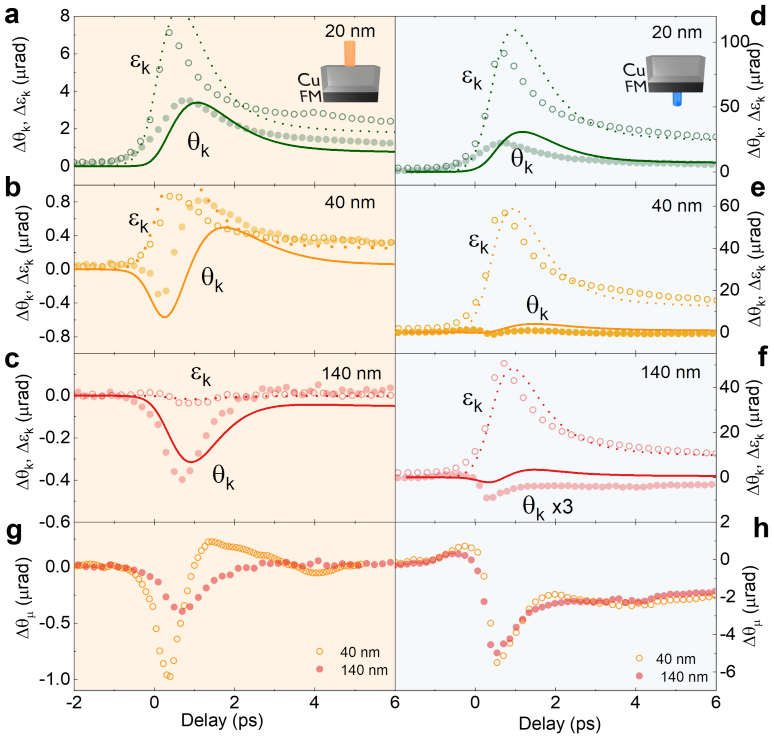

FIG. 3. **Time-resolved magneto-optical signal for rotation and ellipticity and extracted spin accumulation contribution. a-f**. TR-MOKE rotation (filled circles) and ellipticity (open circles) signals for $t_{Cu} \approx 20$, 40, and 140 nm, for both Cu-side (**a,b,c**) and the FM-side (**d,e,f**) probing configurations. Solid and dashed lines are simulations[34] with a single set of magnetic, thermal and optical parameters, except for the fluence which was modified between Cu-side and FM-side experiments.**g-h**. Extracted spin accumulation contribution to the magneto-optical signal ($\Delta\theta_\mu$) from the ellipticity and rotation signals (see text for details).

tically different from that in transition metal ferromagnets.

Multi-physics model: In order to verify the origin of these observed signals we developed a model[34] to estimate the ultrafast demagnetization in the low fluence limit, predict time-dependent spin density profiles and extract the resulting magneto-optical signals. In order to estimate the demagnetization, we first coupled an optical absorption transmission matrix model [58] and 3 temperature model[8] to predict phonon, electron and spin temperatures. By assuming a phenomenological (spin) temperature dependence of the magnetization, we could calculate the evolution of the magnetization (see also [34] for more details and other references for the physical values used such as [59]). We then used a simple spin diffusion model, where the source term is proportional to dM/dt, the change in magnetization. Additionally, a small spin-dependent Seebeck effect was added, as described in Ref.[60]. Finally, by setting a Voigt constant for the Cu layer (based on Ref.[55], see also Ref.[34]), we calculate for each time-step the resulting $\Delta\theta_k$ and $\Delta\epsilon_k$, which we convolute with the probe's temporal shape. In

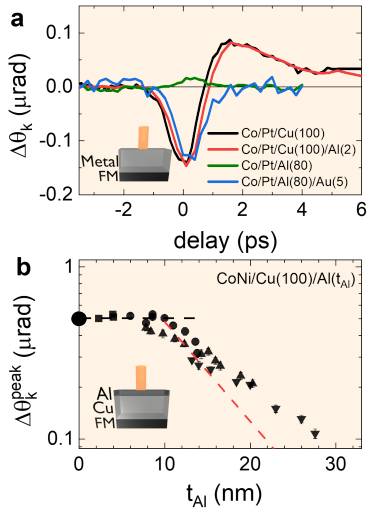

FIG. 4. **Impact of different capping layers in the spin accumulation signal.** **a** TR-MOKE signal from the Cu side with different capping layers. The common part of the stacks is sapphire//Ta(3)/Pt(10)/[Co(0,82)/Pt(1)]$_2$/Co(0,82) abbreviated as Co/Pt. The different samples are , Co/Pt//Cu(100)/Al(2.5), Co/Pt//Al(80) and Co/Pt//Al(80)/Au(5). **b** Scaling of the spin accumulation peak with the thickness of an Al capping layer measured on various wedges covering the range from 0 to 30 nm. The red dashed line corresponds to the Beer-Lambert-like law $e^{-2\pi\lambda^{-1}\mathrm{k_{Al}}2t_{Al}}$, with $\mathrm{k_{Al}} = 8.5$ being Al's optical index imaginary part [53].

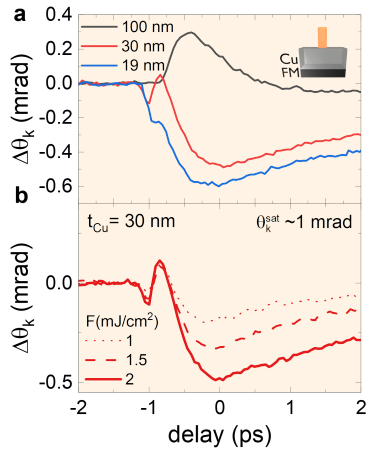

FIG. 5. **High peak power time-resolved magneto-optical signal.** Dependence of the TR-MOKE signal in CoNi/Cu(100) using the amplified laser system (see End Matter) for **a** different Cu thicknesses at a constant fluence of 2 mJ/cm^2 and for **b** different fluences at constant thickness of t_{Cu}=30 nm. A similar behavior is observed in the TR-MOKE signal when compared to the low-energy laser system as seen in Figure 2 at lower fluence, showing a demagnetization-dominated curve at lower t_{Cu} and a spin accumulation-dominated curve at high t_{Cu}, while a mixed state is observed at t_{Cu}=30 nm. As we increase the fluence, we observe that the spin accumulation peak increases along with the demagnetization.

the end, for a given set of parameters, we are able to fit all 12 curves in Figs.**3** corresponding to various samples and probing directions, shown as solid (for $\Delta\theta_k$) or dashed (for $\Delta\epsilon_k$) lines. $\Delta\epsilon_k$ is mostly sensitive to the magnetization dynamics, and results in rather good fits, giving confidence in the estimated dM/dt. $\Delta\theta_k$, which is also sensitive to spin accumulation, is reasonably well fitted too. The relative amplitudes of the signals and the main features such as polarities of the curves are well described, but not all details are captured by the model. Given the large number of layers and parameters, it is difficult to quantify the injected spin density, but with the used parameters we estimate peaks spin densities at the top Cu surface of around 5 A/m. We note that our model does not include sensitivity to spin accumulation within the buffer layers (Ta/Cu) or ferromagnet itself, which could potentially play an important role. This will be addressed in future work.

Finally, by assuming that the magneto-optical signal from Co/Ni and Cu layers is additive, we can extract pure spin accumulation Kerr signal $\Delta\theta_\mu$ traces from the experimental data by the following operation $\Delta\theta_\mu =$

$\theta_k^{sat}(\Delta\theta_k/\theta_k^{sat} - \Delta\epsilon_k/\epsilon_k^{sat})$ and as plotted in Figs.3.g-h. This method allows one to extract spin accumulations for thinner Cu layers, even when signals are somewhat mixed.

The possibility of measuring spin-accumulation through a ferromagnet is certainly not limited to the studied structure. As long as light can penetrate past the magnetic layer, that significant magneto-optical sensitivity exists at the used wavelength in the non-magnetic layers, and that the signals due to spin accumulation can be properly separated from the underlying magnetization dynamics of the magnetic layer (i.e. due to different magneto-optical constants), we believe this method should be universally applicable to any magnet/non-magnetic metal system. In future work, in order to verify the contribution of the spin accumulation within the ferromagnet to the magneto-optical signal, one would need to carefully study single ferromagnetic layers surrounded by insulating layers, such as in Ref.[19] where an accumulation-like peaked signal was also extracted at short timescales from the difference between normalized rotation and ellipticities. In this work, we have mostly fixed the wavelength and chosen to systematically modify the structures, but an alternative powerful method could exploit the spectral sensitivity to magnetization and spin accumulations in the various layers.

—

Discussion: At this point, one might wonder about the origin of the Kerr signal. We first turn our attention to the top Cu/air interface, and investigate its role by modifying the capping. Here we use Co/Pt as the ferromagnet, which results in a rather bipolar spin accumulation signal, as previously shown [28]. We first compare the signal from a bare 100 nm Cu layer (self-passivated) with one capped by 2.5 nm of (self-passivated) Al, but observe no differences (black vs red in Fig.**4**.a). Pt and Ta cappings resulted[34] in a reduction of $\Delta\theta_k$, as reported in [32]. We then verify the possible signal due to the presence of metallic Al (green in Fig.**4**.a) but observed a complete loss of the signal[28]. As a last test, shown in Fig.**4**.b, we increased the thickness of the Al capping, from 2.5 nm to 30 nm, to make sure the Cu layer was not oxidized at all. Indeed, from atomic force microscopy measurements[34] we know that the thick Cu has a roughness of 3 nm for 150 nm Cu films, which could potentially enable oxidation of the Cu even with the thin capping. As the cap thickness is increased, initially no change in the signal is observed, up to around 8 nm, where the signal starts to drop. We attribute the reduction in signal to the fact that the Al layer self-passivates up to a certain thickness (potentially around 8 nm on our very rough layers) and the rest of the aluminum stays metallic. Therefore, the metallic Al layer, which doesn't contribute to MOKE rotation, blocks the probe from reaching the sensitive Cu layer (red fit corresponds to $e^{-4\pi\lambda^{-1}\mathrm{k_{Al}}t_{Al}}$, with $\mathrm{k_{Al}} = 8.5$ being Al's optical index imaginary part [53]. However, this fit over-estimates the loss in signal, which means the metallic Al likely enhances somehow the resulting magneto-optical signal. Nevertheless, it appears that the oxidation state of the Cu interface doesn't play a big role in the magneto-optical detection of spin-accumulation. This result suggests a bulk-sensitivity. This interpretation is strongly backed by our simulations, which only include bulk sensitivity and fit qualitatively well the data in Fig.3.

We note that, interestingly, adding a few nanometers of Au on top of the thick Al(80) layer recovers the Kerr signal (blue in Fig.**4**.a), even though the dynamics are different to those in Cu, probably due to the differences in optical absorption and thermal transport between Cu and Al[61].

Finally, even-though we have only considered spin in our discussion and analysis, one may wonder if the reported signals could be of orbital origin instead[7, 62]. Moreover, magneto-optics are particularly sensitive to orbital angular momentum, without requiring spin-orbit coupling, unlike for sensing spin [7]. We do believe that,

if present, orbital currents may be addressable and distinguishable from spin by these optical methods, by designing the right multilayer and experimental protocol. However, this goes beyond the scope of the present work.

High-fluence experiments: Given the importance of ultrafast spin transport for technological applications, we decided to extend our studies to higher fluence regimes, accessible with most amplified laser systems, and necessary for high intensity THz emission[12] and all-optical switching[9, 11]. To this aim, we used an amplified Ti:Sa laser (see End Matter) to induce large spin dynamics on the same Co/Ni films and detect θ_k. In Fig.**5.a** we show $\Delta\theta_k$ for various Cu thicknesses when probing the Cu-side and pumping the FM-side with 2 mJ/cm^2. As in previous low intensity experiments, we see a transition from a pure demagnetization-like trace, to a mixed one, and to a full spin-accumulation one, for $t_{Cu} \approx 19$, 30 and 100 nm respectively (for a discussion on delays see End Matter). In Fig.**5.b** we show experiments at a fixed thickness of 30 nm, but with increasing fluence, reaching demagnetizations of around 20, 35 and 50% for 1, 1.5 and 2 mJ/cm^2 respectively. Both the demagnetization trace and the spin accumulation increase proportionally to the absorbed fluence, but because the baseline of the spin accumulation peak is being reduced (due to the demagnetization signal), the peak appears at the same position for all fluences. When pushed to the limit, for nearly full demagnetization conditions and for a thickness of around 50 nm (where spin accumulation signals are the largest), we can reach spin accumulation signals on the order of 0.5 mrad. Such θ_k are comparable to the full $\Delta\theta_k$ obtained from thin ferromagnets (see Fig.**1.e-f** or Refs [27, 63] and even thick Fe films[64]. Even if this value is not directly comparable, due to different Voigt constants in each case, it is remarkable that a non magnetic film can be polarized to such an extent by its magnetic Co/Ni neighbor.

CONCLUSION

Our work demonstrates that ultrafast spin accumulations can lead to large magneto-optical signals, at times comparable or larger than the magneto-optical signal originating from magnetic layers. We show that for the case of Cu at a wavelength of 785 nm, spin accumulation induces mainly a Kerr rotation and negligible ellipticity, which can be leveraged to extract the pure demagnetization and spin accumulation temporal profiles for any Cu thickness, even when probed through the ferromagnetic layer. Finally, we show that amplified systems can also be used for these kind of experiments, resulting in up to >0.5 mrad Kerr rotation signals. Our conclusions are backed by simulations combining ultrafast heat and spin-diffusion with a magneto-optical transmission matrix method. This work shows that with proper care, time-resolved magneto-optical experiments become a unique tool to offer a direct view into the ultrafast spin (and/or orbital) transport. Our work is a reminder that care should be taken when interpreting time-resolved magneto-optical traces, particularly when the static magneto-optical signals are low and sensitivities to transient angular momentum in other layers can take over. These developments may prove crucial for the understanding and development of all-optical switching in spin-valves[9] or THz emission in thin multilayers[12, 62].

ACKNOWLEDGEMENTS

This work was supported by the France 2030 government investment plan managed by the French National Research Agency under grant references PEPR SPIN – TOAST ANR-22-EXSP-0003 and SPINMAT ANR-22-EXSP-0007. This work was also supported by the French PIA project “Lorraine Université d’Excellence”, reference ANR-15-IDEX-04-LUE. The project was also supported by project ANR-23-CE30-0047. Alberto Anadón acknowl-

edges the project 3D-Sky (GAP-101108063), part of the Marie Skłodowska-Curie Actions from the Horizon Europe Program of the EU. Views and opinions expressed are those of the author(s) only and do not necessarily reflect those of the European Union. Neither the European Union nor the granting authority can be held responsible for them.

DATA AVAILABILITY

Data is available from the authors upon reasonable request.

* alberto.anadon@inma.unizar-csic.es; These authors contributed equally to this work
† These authors contributed equally to this work
‡ jon.gorchon@univ-lorraine.fr

[1] Y. K. Kato, R. C. Myers, A. C. Gossard, and D. D. Awschalom, Observation of the Spin Hall Effect in Semiconductors, Science **306**, 1910–1913 (2004).

[2] I. Mihai Miron, G. Gaudin, S. Auffret, B. Rodmacq, A. Schuhl, S. Pizzini, J. Vogel, and P. Gambardella, Current-driven spin torque induced by the Rashba effect in a ferromagnetic metal layer, Nature Materials **9**, 230–234 (2010).

[3] G. S. D. Beach, C. Nistor, C. Knutson, M. Tsoi, and J. L. Erskine, Dynamics of field-driven domain-wall propagation in ferromagnetic nanowires, Nature Materials **4**, 741–744 (2005).

[4] M. Yamanouchi, D. Chiba, F. Matsukura, and H. Ohno, Current-induced domain-wall switching in a ferromagnetic semiconductor structure, Nature **428**, 539–542 (2004).

[5] Y. Liu, J. Besbas, Y. Wang, P. He, M. Chen, D. Zhu, Y. Wu, J. M. Lee, L. Wang, J. Moon, N. Koirala, S. Oh, and H. Yang, Direct visualization of current-induced spin accumulation in topological insulators, Nature Communications **9**, 2492 (2018).

[6] C. Stamm, C. Murer, M. Berritta, J. Feng, M. Gabureac, P. M. Oppeneer, and P. Gambardella, Magneto-optical detection of the spin hall effect in pt and w thin films, Phys. Rev. Lett. **119**, 087203 (2017).

[7] Y.-G. Choi, D. Jo, K.-H. Ko, D. Go, K.-H. Kim, H. G. Park, C. Kim, B.-C. Min, G.-M. Choi, and H.-W. Lee, Observation of the orbital Hall effect in a light metal Ti, Nature **619**, 52–56 (2023).

[8] E. Beaurepaire, J.-C. Merle, A. Daunois, and J.-Y. Bigot, Ultrafast spin dynamics in ferromagnetic nickel, Physical review letters **76**, 4250 (1996).

[9] J. Igarashi, W. Zhang, Q. Remy, E. Díaz, J.-X. Lin, J. Hohlfeld, M. Hehn, S. Mangin, J. Gorchon, and G. Malinowski, Optically induced ultrafast magnetization switching in ferromagnetic spin valves, Nature Materials **22**, 725–730 (2023).

[10] G. Malinowski, F. Dalla Longa, J. H. H. Rietjens, P. V. Paluskar, R. Huijink, H. J. M. Swagten, and B. Koopmans, Control of speed and efficiency of ultrafast demagnetization by direct transfer of spin angular momentum, Nature Physics **4**, 855–858 (2008).

[11] I. Radu, K. Vahaplar, C. Stamm, T. Kachel, N. Pontius, H. Dürr, T. Ostler, J. Barker, R. Evans, R. Chantrell, *et al.*, Transient ferromagnetic-like state mediating ultrafast reversal of antiferromagnetically coupled spins, Nature **472**, 205–208 (2011).

[12] T. Seifert, S. Jaiswal, U. Martens, J. Hannegan, L. Braun, P. Maldonado, F. Freimuth, A. Kronenberg, J. Henrizi, I. Radu, E. Beaurepaire, Y. Mokrousov, P. M. Oppeneer, M. Jourdan, G. Jakob, D. Turchinovich, L. M. Hayden, M. Wolf, M. Münzenberg, M. Kläui, and T. Kampfrath, Efficient metallic spintronic emitters of ultrabroadband terahertz radiation, Nature Photonics **10**, 483–488 (2016).

[13] E. Beaurepaire, G. M. Turner, S. M. Harrel, M. C. Beard, J.-Y. Bigot, and C. A. Schmuttenmaer, Coherent terahertz emission from ferromagnetic films excited by femtosecond laser pulses, Applied Physics Letters **84**, 3465–3467 (2004), https://pubs.aip.org/aip/apl/article-pdf/84/18/3465/18588353/3465_1_online.pdf.

[14] R. Rouzegar, L. Brandt, L. c. v. Nádvorník, D. A. Reiss, A. L. Chekhov, O. Gueckstock, C. In, M. Wolf, T. S. Seifert, P. W. Brouwer, G. Woltersdorf, and T. Kampfrath, Laser-induced terahertz spin transport in magnetic nanostructures arises from the same force as ultrafast demagnetization, Phys. Rev. B **106**, 144427 (2022).

[15] B. Pfau, S. Schaffert, L. Müller, C. Gutt, A. Al-Shemmary, F. Büttner, R. Delaunay, S. Düsterer, S. Flewett, R. Frömter, J. Geilhufe, E. Guehrs, C. Günther, R. Hawaldar, M. Hille, N. Jaouen, A. Kobs, K. Li, J. Mohanty, H. Redlin, W. Schlotter, D. Stickler, R. Treusch, B. Vodungbo, M. Kläui, H. Oepen, J. Lüning, G. Grübel, and S. Eisebitt, Ultrafast optical demagnetization manipulates nanoscale spin structure in domain walls, Nature Communications **3**, 1100 (2012).

[16] C. Boeglin, E. Beaurepaire, V. Halté, V. López-Flores, C. Stamm, N. Pontius, H. A. Dürr, and J.-Y. Bigot, Distinguishing the ultrafast dynamics of spin and orbital moments in solids, Nature **465**, 458–461 (2010).

[17] M. Lisowski, P. A. Loukakos, A. Melnikov, I. Radu, L. Ungureanu, M. Wolf, and U. Bovensiepen, Femtosecond electron and spin dynamics in gd(0001) studied by time-resolved photoemission and magneto-optics, Physical Review Letters **95**, 137402 (2005).

[18] B. Koopmans, M. van Kampen, J. T. Kohlhepp, and W. J. M. de Jonge, Ultrafast Magneto-Optics in Nickel: Magnetism or Optics?, Physical Review Letters **85**, 844–847 (2000).

[19] L. Guidoni, E. Beaurepaire, and J.-Y. Bigot, Magneto-optics in the Ultrafast Regime: Thermalization of Spin Populations in Ferromagnetic Films, Physical Review Letters **89**, 017401 (2002).

[20] T. Kampfrath, R. G. Ulbrich, F. Leuenberger, M. Münzenberg, B. Sass, and W. Felsch, Ultrafast magneto-optical response of iron thin films, Phys. Rev. B **65**, 104429 (2002).

[21] B. Koopmans, M. van Kampen, and W. J. M. de Jonge, Experimental access to femtosecond spin dynamics, Journal of Physics: Condensed Matter **15**, S723 (2003).

[22] M. van Kampen, C. Jozsa, J. T. Kohlhepp, P. LeClair, L. Lagae, W. J. M. de Jonge, and B. Koopmans, All-optical probe of coherent spin waves, Phys. Rev. Lett. **88**, 227201 (2002).

[23] G. P. Zhang, W. Hübner, G. Lefkidis, Y. Bai, and T. F. George, Paradigm of the time-resolved magneto-optical Kerr effect for femtosecond magnetism, Nature Physics **5**, 499–502 (2009).

[24] K. Carva, M. Battiato, and P. M. Oppeneer, Is the controversy over femtosecond magneto-optics really solved?, Nature Physics **7**, 665–665 (2011).

[25] J. Wieczorek, A. Eschenlohr, B. Weidtmann, M. Rösner, N. Bergeard, A. Tarasevitch, T. O. Wehling, and U. Bovensiepen, Separation of ultrafast spin currents and spin-flip scattering in co/cu(001) driven by femtosecond laser excitation employing the complex magneto-optical kerr effect, Phys. Rev. B **92**, 174410 (2015).

[26] I. Razdolski, A. Alekhin, U. Martens, D. Bürstel, D. Diesing, M. Münzenberg, U. Bovensiepen, and A. Melnikov, Analysis of the time-resolved magneto-optical kerr effect for ultrafast magnetization dynamics in ferromagnetic thin films, Journal of Physics: Condensed Matter **29**, 174002 (2017).

[27] G.-M. Choi, B.-C. Min, K.-J. Lee, and D. G. Cahill, Spin current generated by thermally driven ultrafast demagnetization, Nature Communications **5**, 4334 (2014).

[28] G.-M. Choi and D. G. Cahill, Kerr rotation in Cu, Ag, and Au driven by spin accumulation and spin-orbit coupling, Physical Review B **90**, 214432 (2014).

[29] G.-M. Choi, C.-H. Moon, B.-C. Min, K.-J. Lee, and D. G. Cahill, Thermal spin-transfer torque driven by the spin-dependent Seebeck effect in metallic spin-valves, Nature Physics **11**, 576–581 (2015).

[30] A. Melnikov, I. Razdolski, T. O. Wehling, E. T. Papaioannou, V. Roddatis, P. Fumagalli, O. Aktsipetrov, A. I. Lichtenstein, and U. Bovensiepen, Ultrafast transport of laser-excited spin-polarized carriers in Au/Fe/MgO(001), Phys. Rev. Lett. **107**, 076601 (2011).

[31] V. H. Ortiz, S. Coh, and R. B. Wilson, Magneto-optical kerr spectra of gold induced by spin accumulation, Phys. Rev. B **106**, 014410 (2022).

[32] G.-M. Choi, Magneto-Optical Kerr Effect Driven by Spin Accumulation on Cu, Au, and Pt, Applied Sciences **8**, 1378 (2018).

[33] M. Hofherr, P. Maldonado, O. Schmitt, M. Berritta, U. Bierbrauer, S. Sadashivaiah, A. J. Schellekens, B. Koopmans, D. Steil, M. Cinchetti, B. Stadtmüller, P. M. Oppeneer, S. Mathias, and M. Aeschlimann, Speed and efficiency of femtosecond spin current injection into a nonmagnetic material, Phys. Rev. B **96**, 100403 (2017).

[34] (), for details refer to the supplementary information.

[35] J. Pudell, M. Mattern, M. Hehn, G. Malinowski, M. Herzog, and M. Bargheer, Heat

Transport without Heating?—An Ultrafast X-Ray Perspective into a Metal Heterostructure, Advanced Functional Materials **30**, 2004555 (2020).

[36] K.-M. Lee, J. W. Choi, J. Sok, and B.-C. Min, Temperature dependence of the interfacial magnetic anisotropy in w/cofeb/mgo, AIP Advances **7**, 065107 (2017), https://pubs.aip.org/aip/adv/article-pdf/doi/10.1063/1.4985720/12882602/065107_1_online.pdf.

[37] D. H. Suzuki and G. S. D. Beach, Measurement of Kerr rotation and ellipticity in magnetic thin films by MOKE magnetometry, Journal of Applied Physics **135**, 063901 (2024), https://pubs.aip.org/aip/jap/article-pdf/doi/10.1063/5.0185341/19583957/063901_1_5.0185341.pdf.

[38] I. H. Malitson and M. Dodge, Refractive Index and Birefringence of Synthetic Sapphire, J. Opt. Soc. Am. **62**, 1405 (1972).

[39] H. Jang, J. Kimling, and D. G. Cahill, Nonequilibrium heat transport in Pt and Ru probed by an ultrathin Co thermometer, Physical Review B **101**, 064304 (2020).

[40] P. B. Johnson and R. W. Christy, Optical Constants of the Noble Metals, Physical Review B **6**, 4370–4379 (1972).

[41] M. Lalieu, R. Lavrijsen, R. A. Duine, and B. Koopmans, Investigating optically excited terahertz standing spin waves using non-collinear magnetic bilayers, Phys. Rev. B **99**, 184439 (2019).

[42] P. Johnson and R. Christy, Optical constants of transition metals: Ti, V, Cr, Mn, Fe, Co, Ni, and Pd, Physical Review B **9**, 5056–5070 (1974).

[43] N. Bergeard, M. Hehn, S. Mangin, G. Lengaigne, F. Montaigne, M. L. M. Lalieu, B. Koopmans, and G. Malinowski, Hot-electron-induced ultrafast demagnetization in Co/Pt multilayers, Phys. Rev. Lett. **117**, 147203 (2016).

[44] G.-M. Choi, D.-K. Lee, K.-J. Lee, and H. W. Lee, Coherent spin waves driven by optical spin-orbit torque, Physical Review B **102**, 014437 (2020).

[45] A. Hubert and R. Schäfer, *Magnetic Domains The Analysis of Magnetic Microstructures* (Springer, 1998).

[46] C.-Y. You and S.-C. Shin, Generalized analytic formulae for magneto-optical Kerr effects, Journal of Applied Physics **84**, 541–546 (1998), https://pubs.aip.org/aip/jap/article-pdf/84/1/541/19020213/541_1_online.pdf.

[47] J. Zak, E. R. Moog, C. Liu, and S. D. Bader, Magneto-optics of multilayers with arbitrary magnetization directions, Phys. Rev. B **43**, 6423–6429 (1991).

[48] R. Atkinson, S. Pahirathan, I. Salter, P. Grundy, C. Tatnall, J. Lodder, and Q. Meng, Fundamental optical and magneto-optical constants of Co/Pt and CoNi/Pt multilayered films, Journal of Magnetism and Magnetic Materials **162**, 131–138 (1996).

[49] J. Kimling, A. Philippi-Kobs, J. Jacobsohn, H. P. Oepen, and D. G. Cahill, Thermal conductance of interfaces with amorphous SiO 2 measured by time-resolved magneto-optic Kerr-effect thermometry, Phys. Rev. B **95**, 184305 (2017).

[50] K. Uchida, S. Takahashi, K. Harii, J. Ieda, W. Koshibae, K. Ando, S. Maekawa, and E. Saitoh, Observation of the spin Seebeck effect., Nature **455**, 778–81 (2008).

[51] A. Slachter, F. L. Bakker, J. P. Adam, and B. J. Van Wees, Thermally driven spin injection from a ferromagnet into a non-magnetic metal, Nature Physics **6**, 879–882 (2010).

[52] (), in some other similar samples a perfect coincidence was found between the dm/dt peak and the spin-accumulation peak when probing the FM-side. We have not yet understood the origin of the delay or lack of it yet between these samples.

[53] M. A. Ordal, R. J. Bell, R. W. Alexander, L. A. Newquist, and M. R. Querry, Optical properties of al, fe, ti, ta, w, and mo at submillimeter wavelengths, Appl. Opt. **27**, 1203–1209 (1988).

[54] We note a little bump in the data at around 4 ps, best visible on the 20 nm sample, which we attribute to a small back reflection of the pump on the sapphire/air interface (delay corresponds to a return trip through the substrate) which induces a second demagnetization.

[55] L. Uba, S. Uba, and V. N. Antonov, Magneto-optical Kerr spectroscopy of noble metals, Physical Review B **96**, 235132 (2017).

[56] A. Mackintosh and O. Andersen, Electrons at the fermi surface, ed. M. Springford, Cambridge Univ. Press, London , 149 (1980).

[57] C. E. Moore, *Atomic Energy Levels: 1H-23V*, Vol. 1 (US Department of Commerce, National Bureau of Standards, 1949).

[58] E. Hecht, *Optics, 4th edition* (Addison-Wesley, 2002).

[59] J. Kimling, J. Kimling, R. B. Wilson, B. Hebler, M. Albrecht, and D. G. Cahill, Ultrafast demagnetization of fept:cu thin films and the role of magnetic heat capacity, Phys Rev. B **90**, 224408 (2014).

[60] G.-M. Choi, C.-H. Moon, B.-C. Min, K.-J. Lee, and D. G. Cahill, Thermal spin-transfer torque driven by the spin-dependent Seebeck effect in metallic spin-valves, Nature Physics **11**, 576–581 (2015).

[61] Similarly, a 200% enhancement of $\Delta\theta_k$ was reported by Choi et al.[32] when a Au capping layer was added on top of Cu.

[62] T. S. Seifert, D. Go, H. Hayashi, R. Rouzegar, F. Freimuth, K. Ando, Y. Mokrousov, and T. Kampfrath, Time-domain observation of ballistic orbital-angular-momentum currents with giant relaxation length in tungsten, Nature Nanotechnology **18**, 1132–1138 (2023).

[63] K. Jhuria, J. Hohlfeld, A. Pattabi, E. Martin, A. Y. Arriola Córdova, X. Shi, R. Lo Conte, S. Petit-Watelot, J. C. Rojas-Sanchez, G. Malinowski, S. Mangin, A. Lemaître, M. Hehn, J. Bokor, R. B. Wilson, and J. Gorchon, Spin–orbit torque switching of a ferromagnet with picosecond electrical pulses, Nature Electronics **3**, 680–686 (2020).

[64] J. Zak, E. Moog, C. Liu, and S. Bader, Universal approach to magneto-optics, Journal of Magnetism and Magnetic Materials **89**, 107–123 (1990).

[65] N. Stojanovic, D. H. S. Maithripala, J. M. Berg, and M. Holtz, Thermal conductivity in metallic nanostructures at high temperature: Electrons, phonons, and the wiedemann-franz law, Phys. Rev. B **82**, 075418 (2010).

[66] J. Pudell, A. Maznev, M. Herzog, M. Kronseder, C. H. Back, G. Malinowski, A. von Reppert, and M. Bargheer, Layer specific observation of slow thermal equilibration in ultrathin metallic nanostructures by femtosecond x-ray diffraction, Nature communications **9**, 3335 (2018).